2nd Micro and Nano Flows Conference
West London, UK, 1-2 September 2009

Dispersion phenomena in microchannels: Transition from Taylor-Aris to convection-dominated regime

A. Adrover, S. Cerbelli, F. Garofalo, M. Giona*

* Corresponding author: Tel.: ++39 (0)644585892; Email: max@giona.ing.uniroma1.it
Università di Roma "La Sapienza", Dipartimento di Ingegneria Chimica
Via Eudossiana 18, 00184 - Roma, Italy

Abstract This article addresses the qualitative and quantitative properties of solute transport and dispersion in microchannel of finite-length. As the Peclet number increases a transition from the Taylor-Aris to a new regime referred as convection dominated dispersion occurs, which is controlled by the velocity profile near the stagnation points at the solid walls. The properties characterizing dispersion dominated regime can be used for analytical purposes as a chromatographic-based velocimetry and for determining the eventual occurrence of slip at the solid walls of microchannels.

Keywords: Channel Flow, Advection-Diffusion, Dispersion, Slip flow

1. Introduction

Dispersion phenomena in microchannels and microflow devices control the performance of many hydrodynamical and chemical processes in micro-Total Analysis and Lab-on-Chip Systems chemical reactions, microseparations, microchromatographic measurements.

The recent Literature on fluid dispersion in microchannels has been mainly focused on the analysis and prediction of the Taylor-Aris dispersion coefficient, and on the influence of geometric parameters and of cross-sectional flows in the Taylor-Aris dispersion regime [1-4]. In point of fact, Taylor-Aris theory applies to infinitely extended channels, and is not suited for predicting finite-size effects occurring in a microcapillary of finite length.

While the theoretical analysis of dispersion has been mainly focused on very long microchannels, for which the Taylor-Aris dispersion theory applies [1], in recent years *wide-bore chromatography* has been proposed and succesfully applied for resolving small molecules or for the determination of particle size in the nanometer regime [5-7]. By definition, wide-bore chromatography operates with columns and microchannels possessing relatively small length-to-radius aspect ratio $\alpha = L/R \leq 300$, and for very high Peclet number (which is the ratio of the characteristic time scales for diffusion and advection). This is exactly the range of operations for which Taylor-Aris dispersion theory does not apply [8].

In point of fact, a theory for transport and dispersion in wide-bore chromatography is still lacking, and the working region of this analytical technique falls in the no-man's land of dispersion diagrams, where no theoretical results are available. As a consequence the design of these devices rests upon case-by-case numerical studies (see e.g. figure 20.5.2 of a classical reference on transport phenomena [9] based on a classical work on dispersion [10]).

The aim of this article is to address the transition from Taylor-Aris to this new regime, referred to as *convection dominated* regime, and to explore its applications, especially those

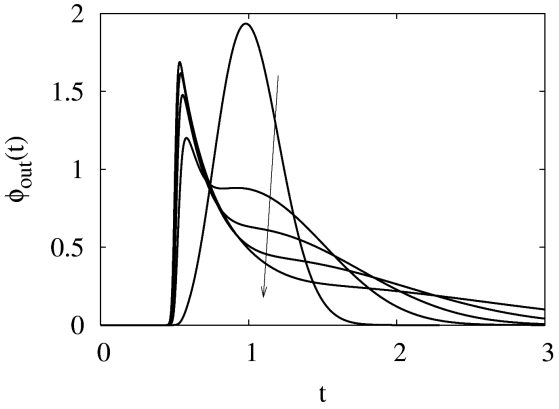

Figure 1:Normalized outlet chromatogram $\phi_{out}(t)$ *vs* t *in a circular cross-section Poiseuille channel at* $\alpha=100$ *for different Peclet values. The arrow indicates increasing values of Peclet* $Pe=10^4$, 5×10^4 , 10^5 , 2×10^5 , 5×10^5 .

concerning chromatographic velocimetry analysis of slip boundary velocity in microchannels.

2. From Taylor-Aris to convection-dominated regime

Consider a cylindrical microcapillary of circular cross-section and finite length L and radius R in which a Poiseuille flow $v_z(r)$ is driven by a pressure drop imposed at the ends of the capillary. The evolution of the concentration of a solute injected into the column is described by the advection-diffusion equation. If the inlet is radially symmetric, the advection-diffusion equation in dimensionless form simplifies as

$$\frac{\partial\phi}{\partial t}=-u(\rho)\frac{\partial\phi}{\partial\zeta}+\frac{1}{Pe}\frac{\partial^2\phi}{\partial\zeta^2}+\frac{\alpha^2}{Pe\,\rho}\frac{\partial}{\partial\rho}\left(\rho\frac{\partial\phi}{\partial\rho}\right) \tag{1}$$

where $\phi(t,\zeta,\rho)$ is the dimensionless solute concentration that depends on the radial coordinate $\rho=r/R$, on the axial coordinate $\zeta=z/L$, and on the dimensionless time t which is the physical rescaled with respect to L/V_{ref} , V_{ref} is the characteristic axial velocity, defined in such a way that the dimensionless velocity $u(\rho)=v_z(R\rho)/V_{ref}$ possesses unit average. Two dimensionless parameters enter eq. (1), namely the Peclet number $Pe=V_{ref}L/D$, where D is solute diffusivity, and the channel aspect ratio $\alpha=L/R$. The initial and boundary conditions for the evolution of the solute concentration are $\phi|_{t=0}=0$, $\phi|_{\zeta=0}=\delta(t)$, that corresponds to an impulsive loading at the inlet section ($\delta(t)$ is the Dirac's delta function), $\partial\phi/\partial\rho|_{\rho=0,1}=0$, and $\partial\phi/\partial\zeta|_{\zeta=1}=0$, expressing the Danckwerts' boundary condition at the outlet section, respectively. The normalized Poiseuille velocity profile is thus $u(\rho)=2(1-\rho^2)$.

As in hydrodynamic chromatography, all the information about solute transport and dispersion within the microchannel can be obtained from the analysis of the average outlet concentration

$$\phi_{out}(t)=2\int_0^1\phi(t,\zeta=1,\rho)\,\rho\,d\rho \tag{2}$$

and of its moments $m_{out}^{(n)}$ defined as

$$m_{out}^{(n)}=\int_0^\infty t^n\phi_{out}(t)\,dt \tag{3}$$

Figure 1 shows the shape of the outlet chromatogram for $\alpha=100$ at increasing values of the Peclet number. These simulations have been obtained by applying both a finite volume and a finite element code. At $Pe=10^4$, one recovers the classical, almost Gaussian-shaped profile, possessing a mode located close to dimensionless flow residence time, i.e. $t=1$. This is the typical chromatogram in the Taylor-Aris regime. As Pe increases further, the modal abscissa t_{mode} (i.e. the peak location) of the chromatogram shifts progressively towards the minimum residence time $t_{min}=1/2$ and attains a highly asymmetric shape. This qualitative change in the shape of the outlet chromatograms is the fingerprint of a transition in the transport regime occurring within the cylindrical capillary, which can be further quantified by considering the first moment and the outlet variance .

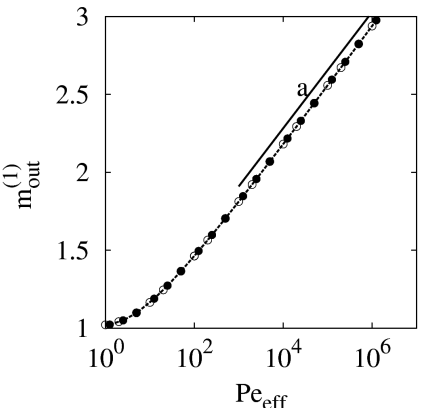

Figure 2(A): $m^{(1)}_{out}$ *vs* Pe_{eff} *. Symbols* ○ *and* ● *refer to* $\alpha=20$ *and* $\alpha=100$ *, respectively. Line (a) represents scaling* $m^{(1)} \sim A\log(Pe_{eff})$ *with* $A=0.162$ *.*

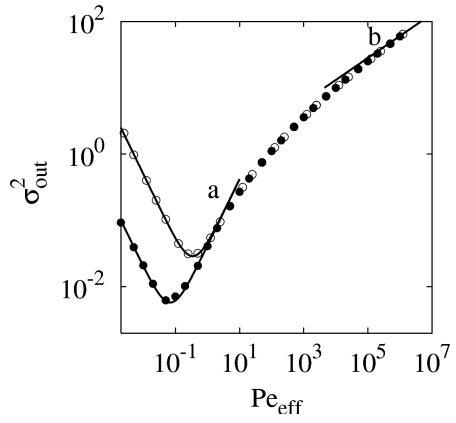

Figure 2(B): σ^2_{out} *vs* Pe_{eff} *. Symbols* ○ *and* ● *refer to* $\alpha=20$ *and* $\alpha=100$ *, respectively. Line (a) represents the Taylor-Aris prediction eq. (5), line (b) is the scaling* $\sigma^2_{out} \sim Pe^{1/3}$ *.*

Figure 2 panels (A) and (B) depict the behaviour of $m^{(1)}_{out}$ and $\sigma^2_{out} = m^{(2)}_{out} - m^{(1)2}_{out}$ as a function of the effective Peclet number Pe_{eff}

$$Pe_{eff} = \frac{Pe}{\alpha^2} \tag{4}$$

which corresponds to the prefactor weighting the contribution of the transverse diffusion in the balance eq. (1).

Consider the variance σ^2_{out} . For $Pe_{eff} \le Pe^*_{eff} \simeq 5$, dispersion can be described by mean of the Taylor-Aris theory, and the outlet variance can be expressed as

$$\sigma^2_{out} = \frac{2}{Pe\,\alpha^2} + \frac{2\,\Gamma_{TA}}{Pe_{eff}} \tag{5}$$

where Γ_{TA} is the Taylor-Aris coefficient, that in cylindrical capillaries equals $\Gamma_{TA} = 1/48$. Lines (a) in figure 2(B) corresponds to the Taylor-Aris variance eq. (5). For $Pe_{eff} > Pe^*_{eff}$, Taylor-Aris predictions fail and a new transport regime sets in in which dispersion phenomena are completely controlled by axial convection. The properties of the convection dominated regime are addressed in the next paragraph.

A further result that emerges from the data of figure 2(A)-(B) is that for $Pe_{eff} > Pe^*_{eff}$ the contribution of axial dispersion is completely negligible. This means that, in the analysis of convection dominated regime, the term $1/Pe\,\partial^2\phi/\partial\zeta^2$ in eq. (1) can be dropped out.

3. Properties of convection-dominated regime

In the Taylor-Aris regime, the nonuniform character of velocity profile contributes to dispersion (second term at the rhs of eq. (5)). This convection-enhanced dispersion is homogeneous in the meaning that each fluid particle explores all the cross section. As a consequence, the resulting concentration profiles in the Taylor-Aris regime approach a Gaussian shape, and the Taylor contribution (second term at the rhs of eq. (5)) is a kind of average of the interplay between axial convection and transverse diffusion over all the channel cross section.

Conversely, convection-enhanced dispersion, occurring for higher Peclet numbers, is a *localized*

phenomenon. In this regime, solute particles do not visit the entire cross section while moving downstream. This phenomenon is depicted in figure 3 (A)-(C), that shows some solute trajectories, obtained by solving the Langevin equations in a 2d channel flow. In figure 3, $0 \le \eta \le 1$ is the normalized transverse coordinate, while $0 \le \zeta \le 1$ is the normalized axial coordinate.

Two implications can be derived from the above observation:

- for $\varepsilon = Pe_{eff}^{-1} \to 0$, the outlet chromatogram approaches the kinematic residence time, that can be obtained by analyzing the statistics of the time of flight $t = 1/u(\rho)$, with respect to a uniform initial location of solute particles at the inlet section;

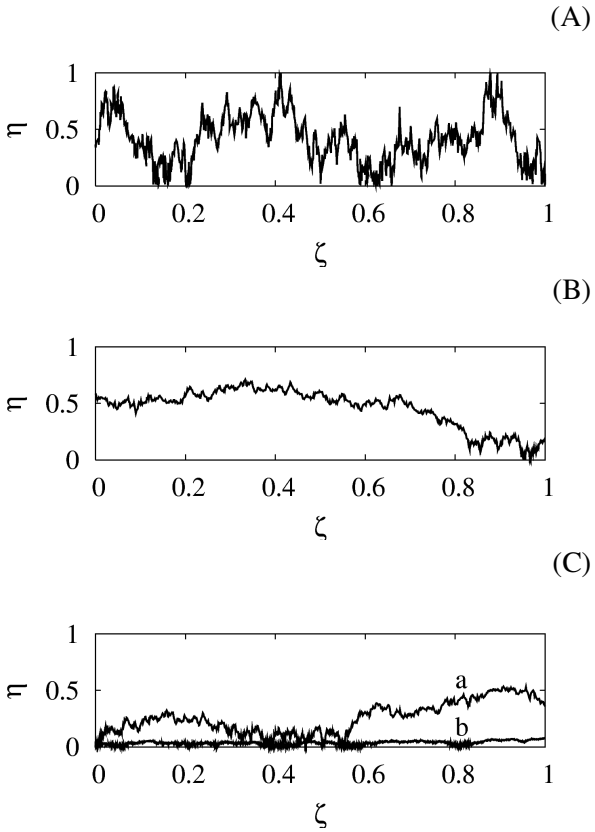

Figure 3: Trajectories of biased Brownian particles within finite length 2d column at $\alpha = 100$ *. (A)* $Pe_{eff} = 0.5$ *,(B)* $Pe_{eff} = 10$ *, (C)* $Pe_{eff} = 10$ *(line a) and* $Pe_{eff} = 10^3$ *(line b) starting from* $\eta = 0$ *.*

- the scaling properties of convection-dominated dispersion are controlled by the dispersion boundary layer, localized close to the velocity stagnation points.

To simplify the analysis consider the case of a 2d Poiseuille flow. Neglecting axial diffusion, the balance equation for nondimensional solute concentration reads

$$\frac{\partial \phi}{\partial t} = -u(\eta)\frac{\partial \phi}{\partial \zeta} + \frac{1}{Pe_{eff}}\frac{\partial^2 \phi}{\partial \eta^2} \qquad (6)$$

where $u(\eta) = 6\eta(1-\eta)$ for a Poiseuille flow. The local moments $m^{(n)}(\zeta, \eta)$ can be introduced,

$$m^{(n)}(\zeta, \eta) = \int_0^\infty t^n \phi(t, \zeta, \eta)\, dt \qquad (7)$$

so that $m_{out}^{(n)} = \int_0^1 m^{(n)}(\zeta = 1, \eta)\, d\eta$.

Figure 4 depicts the structure of the dispersion boundary layers in the case of the 2d Poiseuille flow. From the localization properties of the dispersion boundary layers it is possible to derive a scaling theory for convection dominated dispersion [11]. Beyond the technical details, essentially the theory predicts in a cylindrical Poiseuille flow that:

- the first-order moment diverges logarithmically with the effective Peclet number

$$m_{out}^{(1)} \sim A \log Pe_{eff} \qquad (8)$$

  where A is a constant.
- the outlet variance σ_{out}^2 scales as

$$\sigma_{out}^2 \sim Pe_{eff}^{1/3} \qquad (9)$$

These results are confirmed in the numerical simulations depicted in figure 2 (A)-(B).

Let us briefly discuss the shape of the outlet chromatogram $\phi_{out}(t)$ depicted in figure 5. Up to $t < t_{max}$ the outlet chromatograms follows the kinematic limit $\phi_{out}^{kin}(t)$ which corresponds to the probability density function for the time of flight of

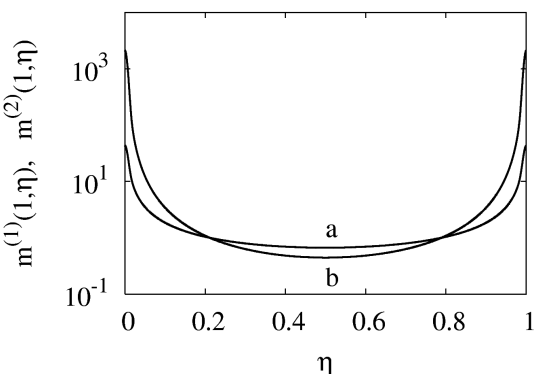

Figure 4:Representation of the dispersion boundary layers for the first (line a) and the second order (line b) moments in a 2d Poiseuille channel at $Pe_{eff}=10^6$.

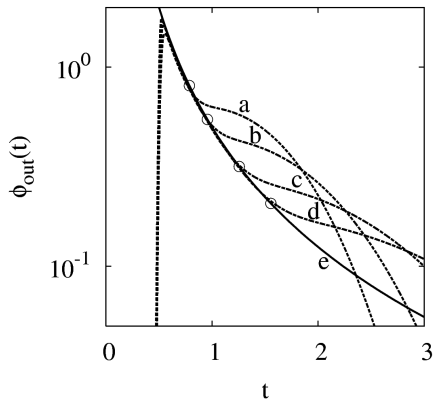

Figure 5:Behaviour of $\phi_{out}(t)$ *vs* t *for a 3d Poiseuille flow in a cylindrical channel. Symbols* ○ *correspond to points at coordinates* $(t_{max}(Pe_{eff}), \phi_{out}^{kin}(t_{max}(Pe_{eff})))$. *Dashed lines (a-d) depict the outlet chromatograms at* $Pe_{eff}=10^1$, 2×10^1 , 5×10^1 , 10^2 , *respectively. Solid line (e) represents the kinematic limit* $\phi_{out}^{kin}(t)=1/(2t^2)$.

solute particle in the absence of diffusion

$$\phi_{out}^{kin}(t)=\begin{cases} 0 & t<1/2 \\ 1/(2t^2) & t>1/2 \end{cases} \qquad (10)$$

The value of t_{max} can be predicted from scaling analysis and equals

$$t_{max}(Pe_{eff})=\frac{Pe_{eff}^{1/3}}{2\,2^{2/3}} \qquad (11)$$

For $t>t_{max}$, the behaviour of ϕ_{out} can be approximated by a Gaussian, centered at t_{max} , with a terminal variance proportional to $Pe_{eff}^{2/3}$.

4. Identification of slip effects and chromatographic velocimetry

Since the convection-dominated regime is strongly sensitive to the shape of the axial velocity field, transport experiments in finite-length channels for high Pe_{eff} (which implies the use of nanoparticles) can be used to infer properties of the velocity field from the analysis of outlet chromatograms. A first application is the possibility of detecting the occurrence of a slip velocity at the microchannels walls. For a slip Poiseuille flow, the normalized velocity field is given by

$$u(\rho)=\frac{2}{1+2\gamma}\left(1+\gamma-\rho^2\right) \qquad (12)$$

where $\gamma=2\ell_s/R$ is the normalized slip length (the physical slip length is ℓ_s). A qualitative transition occurs in the behaviour of the outlet variance for slip and no-slip flows.

For a no-slip flow, σ_{out}^2 diverges to infinity as Pe_{eff} increases, while in the presence of slip σ_{out}^2 saturates towards a constant value that depends on the slip length (see figure 6), which can be predicted from the kinematic limit $\phi_{out}^{kin}(t)$:

$$\lim_{Pe_{eff}\to\infty}\sigma_{out}^2=\int_0^\infty (t-m_{kin}^{(1)})\,\phi_{out}^{kin}(t)\,dt \qquad (13)$$

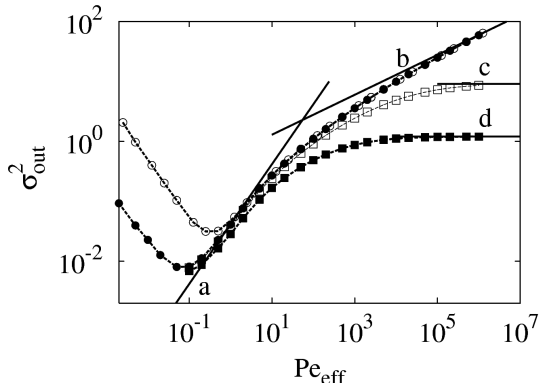

Figure 6: σ^2_{out} *vs* Pe_{eff} *. Symbols* ○ *refer to* $\alpha=20$, ● *to* $\alpha=100$ *in the presence of no slip-velocity profile. Symbols* □ *and* ■ *refer to* $\alpha=100$ *and* $\gamma=0.02$ *and* $\gamma=0.1$ *, respectively. Line (a) is the Taylor-Aris scaling* $\sigma^2(Pe_{eff})=2\mathrm{Pe}_{eff}/48$ *, line (b) is the scaling* $\sigma^2(Pe_{eff})\sim Pe_{eff}^{1/3}$ *. Lines (c) and (d) show the saturation values predicted by kinematic limit.*

being $m^{(1)}_{kin}=\int_0^\infty t\,\phi^{kin}_{out}(t)\,dt$. This provides a fully transport-based approach to predict the occurrence of slip flow in microchannels. A second application, strongly related to the first, is the possibility of using wide-bore chromatography for high values of Pe_{eff} to obtain more comprehensive information on the velocity profile within a channel. This technique, that can be referred to as *chromatographic velocimetry*, is briefly outlined in this section.

Consider first the kinematic residence time distribution $\phi^{kin}_{out}(t)$, and let $p_u(u)$ be the probability density function for the velocity: $p_u(u)du$ is the fraction of fluid particle having velocity in the interval $(u,u+du)$. From the relation between the kinematic residence time t and the velocity u , $t=1/u$, and from an elementary probability balance it follows that

$$p_u(u)=\phi^{kin}_{out}(t)t^2\big|_{t=1/u} \qquad (14)$$

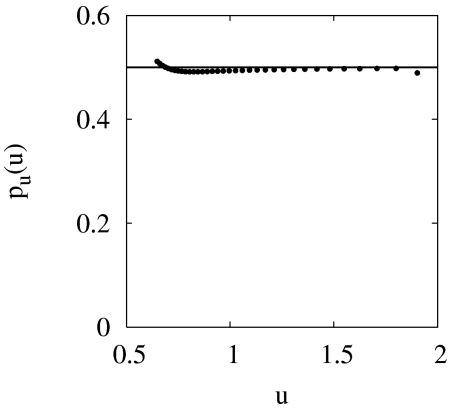

Figure 7:Probability density function $p_u(u)$ *vs* u *for the velocity. Dots are the results of the analysis of the outlet chromatogram for* $Pe_{eff}=10^6$, $\alpha=10^2$ *, the solid horizontal line represents the exact result* $p_u(u)=1/2$.

In the case of the no-slip Poiseuille flow in a cylindrical capillary of circular cross-section, eq. (14) reduces to

$$p_u(u)=\begin{cases}1/2 & 0\le u\le 2\\ 0 & otherwise\end{cases} \qquad (15)$$

Eq. (14) can be generalized to the analysis of chromatographic experiments. Indeed, in the time interval $t_{mode}<t<t_{max}(Pe_{eff})$, which corresponds to the velocity interval $t^{-1}_{max}(Pe_{eff})<u<t^{-1}_{mode}$, the probability density function $p_u(u)$ can be estimated (approximately) from the outlet concentration profile $\phi_{out}(t)$ as

$$p_u(u)\simeq\phi_{out}(t)t^2\big|_{t=1/u} \qquad (16)$$

Figure 7 shows the application of eq. (16) for $Pe_{eff}=10^2$, compared with the analytical result Eq. (15). The velocimetric analysis can be further generalized in the case the axial velocity is a monotonic function of the radial abscissa. Under this hypothesis, it is possible to estimate the velocity profile $u(\rho)$ from a chromatographic

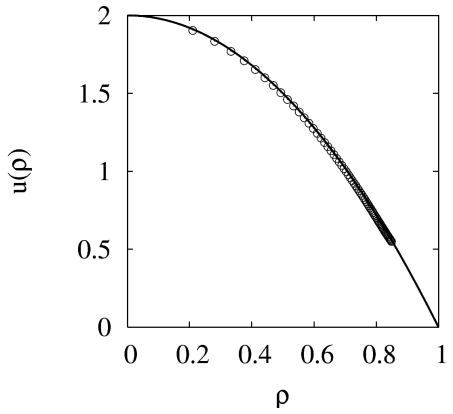

Figure 8:Velocity profile $u(\rho)$ *vs* ρ *(symbols* ○ *) estimated from the outlet chromatogram at* $Pe_{eff}=10^6$, $\alpha=10^2$. *The solid line is the Poiseuille profile* $u(\rho)=2(1-\rho^2)$.

experiments. To show this, let $u=f(\rho)$ be the monotonic velocity profile, and let

$$\rho=f^{-1}(u) \tag{17}$$

be its inverse function. From a probability balance in a cylindrical capillary with circular cross-section, one obtains

$$\int_0^u p_u(u')\,du'=2\int_{f^{-1}(u)}^1 \rho\,d\rho=1-\left[f^{-1}(u)\right]^2 \tag{18}$$

and therefore

$$\rho^2=1-\int_0^u p_u(u')\,du'=1-\int_{1/u}^{\infty}\phi_{out}^{kin}(t')\,dt' \tag{19}$$

This result can be extended to the analysis of chromatographic data, namely

$$\rho=\left[1-\int_{1/u}^{\infty}\phi_{out}(t')\,dt'\right]^{1/2} \tag{20}$$

which applies in the interval $t_{max}^{-1}(Pe_{eff})<u<t_{mode}^{-1}$ and represents the equation for extracting velocimetry data from chromatographic experiments. Figure 8 depicts the application of eq. (20) for $Pe_{eff}=10^6$.

5. Concluding Remark

Whenever finite length microchannels are considered $\alpha\sim10\div300$, transport of slowly diffusing solute particles is characterized by a new regime (referred to as convection-dominated regime) which is completely different from Taylor-Aris dispersion. We have shown numerical results for 2d straight, and 3d cylindrical channels for which $\sigma_{out}^2\sim Pe_{eff}^{1/3}$. By changing the geometry of the cross section it is possible to obtain in the Stokes regime other scaling behaviours. For instance, in rectangular microchannels $\sigma_{out}^2\sim Pe^{1/2}$.

The phenomenology associated with convection-dominated dispersion depends heavily on the structure of boundary layers that become localized close to the stagnation points of the velocity field.

We have shown that wide-bore chromatography can be used for assessing the occurrence of slip flows in microchannels and for deriving information on the velocity profile starting from the behaviour of the outlet chromatogram.

6. Bibliography

1. R. Aris, Proc. R. Soc. London A 235 (1956) 67-77.
2. D. Dutta, A. Ramachandran, D.T. Leighton Jr., Microfluid Nanonfluid 2 (2006) 275-290.
3. A. Ajdari, N. Bontoux, H.A. Stone, Anal. Chem. 78 (2006) 387-392.
4. H. Zhao, H. H. Bau, Anal. Chem. 79 (2007) 7792-7798.
5. T. Okada, M. Harada, T. Kido, Anal. Chem. 77 (2005) 6041-6046.
6. C.-H. Fischer, M.J. Giersig, J. Chromatogr. A 688 (1994) 97–105.
7. M. Harada, T. Kido, T. Masudo, T. Okada, Anal. Sci. 21 (2005) 491–496.
8. J.T. Vanderslice, A.G. Rosenfeld, G. Beecher, Anal. Chim. Acta 179 (1986) 119–1129.
9. R.B. Bird, W.N. Stewart, E.N. Lightfoot, Transport Phenomena, 2nd ed., Wiley: Chichester,

2002.
10. V. Ananthakrishnan, W. Gill, A. Barduhn, AIChE J. 11 (1965) 1063–1072.
11. M. Giona, A. Adrover, S. Cerbelli, F. Garofalo (2009), in preparation.